Journal of Solid State Chemistry **162,** 52–62 (2001)
doi:10.1006/jssc.2001.9340, available online at http://www.idealibrary.com on IDEAL®

Direct Intercalation of Amino Acids into Layered Double Hydroxides by Coprecipitation

Sumio Aisawa, Satoshi Takahashi, Wataru Ogasawara, Yoshio Umetsu, and Eiichi Narita[1]

Department of Chemical Engineering, Faculty of Engineering, Iwate University, 4-3-5 Ueda, Morioka 020-8551, Japan

Received April 30, 2001; in revised form July 17, 2001; accepted August 2, 2001

First, the direct intercalation of amino acids into various layered double hydroxides (Mg–Al, Mn–Al, Ni–Al, Zn–Al, and Zn–Cr LDHs) by coprecipitation has been investigated using phenylalanine (Phe) as a guest amino acid. The degree of Phe coprecipitation was strongly influenced by the solution pH and kind of LDH system and reached a maximum in the pH 8–10 region. The solid products were found to have an expanded LDH structure, which supported the belief that Phe was intercalated into LDHs as an amphoteric ion or anion. Two kinds of configuration for Phe in the gallery, either vertical (Mn–Al, Zn–Al, and Zn–Cr LDHs) or horizontal (Mg–Al LDH) in orientation were observed. Only in the Ni–Al systems, the solid product was the mixture of Phe/Ni–Al LDH and Phe/Ni(OH)$_2$ composite. Next, the thermal decomposition of the intercalated Phe was revealed to be accelerated by the catalytic action of metal ions in the host basal layer. The formation of Phe/Mg–Al, Mn–Al, and Zn–Al LDHs was also elucidated as being appreciably different by the kind of LDH system. Moreover, for various amino acids, the degree of coprecipitation was found to be strongly influenced by amino acid sidechains, i.e., length, structure, and physicochemical properties. © 2001 Academic Press

Key Words: **layered double hydroxide; intercalation; coprecipitation; amino acids; organic–inorganic hybrid materials; thermal decomposition; catalytic action.**

INTRODUCTION

Layered double hydroxides (LDHs) are widely known as host–guest materials, anion exchangers, anionic clays and hydrotalcite-like compounds. LDHs possess a positively charged hydroxide basal layer due to substitution of trivalent cations for part of the divalent cations in the hydroxide basal layer and are electrically balanced by the intercalation of anions into the interlayer space; the remaining interlayer space is occupied by water molecules. LDHs can be represented by $[M^{2+}_{1-x}M^{3+}_{x}(OH)_2]\ [A^{n-}_{x}/n \cdot yH_2O]$, where M^{2+} and M^{3+} represent metallic cations such as Mg^{2+}, Ni^{2+}, Mn^{2+}, or Zn^{2+} and Al^{3+}, Cr^{3+}, or Fe^{3+}, etc. A^{n-} is an exchangeable inorganic anion such as CO_3^{2-}, SO_4^{2-}, Cl^-, NO_3^-, or various organic anions, and the x value, i.e., the charge density, is equal to the molar ratio $M^{3+}/(M^{2+}+M^{3+})$ (1–5). Recently, LDHs have received considerable attention due to their potential technological applications such in catalysis, as electrodes as in optical memory, as sensitizers, as separators and as synthesis material for organic–inorganic nanocomposites (6–12).

Synthesis, characterization, and application of organo/LDH composites prepared by the intercalation of organic substances into LDHs have been reviewed (13). Furthermore, there have been several reports on the intercalation of organic substances, e.g., organic carboxylic acid, anionic polymer, cyclodextrin, organic phosphoric acid, and fullerene, into LDHs (14–23). The intercalation of organic substances into LDHs has generally been accomplished by the following methods: anion-exchange (24), reconstruction (25), and coprecipitation (26). In particular, the coprecipitation method has often been used for the direct formation of organo/LDH composites.

Synthesis of biomolecules/LDHs has become of interest in recent years. The intercalation of nucleoside monophosphates and deoxyribonucleic acid into a Mg–Al LDH by the anion-exchange method has been reported (27). The biomolecule intercalated Mg–Al LDH hybrids are expected for the developing new gene reservoir and carrier. On the other hand, regarding amino acids, which are wellknown as components of proteins and of biomolecules, there are few studies on the intercalation of amino acids into LDHs. The intercalation of glutamic acid, aspartic acid, and poly(aspartic acid) into Mg–Al LDH by the coprecipitation method has been reported (28). The intercalation of phenylalanine and tyrosine into a Zn–Al LDH by the ion-exchange method has also been investigated (29). However, quantitative examination is lacking and the intercalation of amphoteric amino acids into LDHs has not been investigated by the coprecipitation method so far. Accordingly, we have previously investigated the quantitative examination of co-

[1]To whom correspondence should be addressed. Fax: + 81-(0)19-621-6331. E-mail: enarita@iwate-u.ac.jp.

0022-4596/01 $35.00

precipitation of phenylalanine into Zn–Al LDH precipitates (30).

In this paper, the intercalation of a variety of amino acids into various kinds of LDHs (Mg–Al, Mn–Al, Ni–Al, Zn–Al, and Zn–Cr systems) has been examined using the coprecipitation method as well as the characterization of the resulting amino acid/LDH composites. Furthermore, the formation process of the phenylalanine/M^{2+}–M^{3+} LDH composite (Mg–Al, Mn–Al, and Zn–Al system) precipitates has also been investigated.

EXPERIMENTAL

Materials

Amino acids and inorganic reagents were purchased from Wako Pure Chemical Industries, Ltd. (Japan), and used without purification.

Coprecipitation of Amino Acids with LDH Precipitates

LDH precipitates were prepared by hydrolysis of M^{2+} and M^{3+} ions in the presence of amino acid. The mixed solution of 1 M $M^{2+}(NO_3)_2$ and $M^{3+}(NO_3)_3$ (M^{2+}/M^{3+}/amino acid molar ratio = 2/1/1, M^{2+}–M^{3+} = Mg–Al, Mn–Al, Ni–Al, Zn–Al, and Zn–Cr) was added dropwise to 50-mM amino acid solution with stirring under a nitrogen atmosphere to avoid contamination by atmospheric CO_2. The solution pH was adjusted by dropwise addition of 1 M NaOH solution, and the temperature was kept at 40°C in a thermostat set. The resulting precipitate was collected by centrifugation after aging for 1 h. The supernatant solution was subjected to measurement of the amino acid concentration by using a Shimadzu TOC-5000 total organic carbon analyzer. The solid product (precipitate) was washed with distilled water and dried in a vacuum oven at 60°C.

In the coprecipitation experiments investigating the formation of the phenylalanine/M^{2+}–M^{3+} LDH (Mg–Al, Mn–Al, and Zn–Al systems) precipitate, a constant volume of the slurry was taken out from the reaction product at proper times. After-treatment of the slurry sample was carried out as that described above.

Characterization of Solid Products

Powder X-ray diffraction (XRD) measurements were performed on a Rigaku Rint 2200 powder X-ray diffractometer, using Cu$K\alpha$ radiation ($\lambda = 0.15401$ nm) at 20 mA, 40 kV, a scanning rate of 2°/min, and a 2θ angle ranging from 2° to 50°. Fourier transform infrared (FT-IR) spectra were obtained using a JASCO WS/IR 7300 FT-IR spectrophotometer by the standard KBr disk method. Thermogravimetry (TG) and differential thermal analysis (DTA) were carried out in the temperature range 30–800°C in flowing air at a heating rate of 10°C/min using a Seiko TG/DTA 320 instrument. Scanning electron micrographs (SEM) were obtained using a Hitachi S-2250 scanning electron microscope. Chemical analysis data for the solid products were determined using a Hitachi 180-80 atomic adsorption spectrometer (metal ion), TOA Electronics IA-100 ion analyzer (NO_3^- ion), and Shimadzu TOC-5000 total organic carbon analyzer (amino acid), respectively.

RESULTS AND DISCUSSION

Coprecipitation Behavior of Phenylalanine with Various LDH Precipitates

In this section, the coprecipitation behavior of amino acid with the various LDH precipitates was investigated using phenylalanine (Phe) as a guest amino acid because of its having a nonpolar phenyl group as a sidechain, which is convenient for simplifying the interaction between the host hydroxide layer and the guest amino acid. The influence of the solution pH on the Phe coprecipitation was investigated with various LDHs precipitates, and the results are shown in Fig. 1. The precipitation pH of various hydroxides was calculated from K_{sp} values as follows: $Mg(OH)_2 = 8.6$, $Ni(OH)_2 = 5.4$, $Mn(OH)_2 = 7.6$, $Zn(OH)_2 = 5.5$, $Al(OH)_3 = 3.4$, and $Cr(OH)_3 = 3.9$ (M^{2+} and M^{3+} concentration is 1 M). The degree of Phe coprecipitation was affected both by the solution pH and by the kind of LDH systems, indicating the following order: Ni–Al > Zn–Al > Mn–Al > Zn–Cr > Mg–Al. In the Ni–Al system, the highest degree of Phe coprecipitation was observed in the wide range pH 6–10, being different from other systems. In the Mn–Al, Zn–Al, and Zn–Cr systems, the degree of Phe coprecipitation reached a maximum in the pH 8–9 range in which most of the Phe exist in amphoteric ion form, because the acid–base equilibrium constants of Phe are $pK_1 = 2.16$ and $pK_2 = 9.18$. Chemical compositional data on the solid

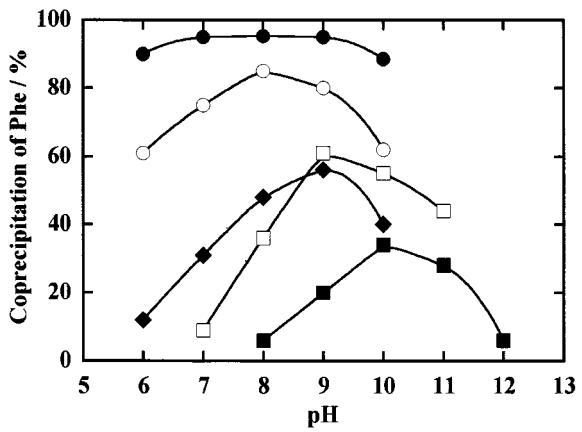

FIG. 1. Influence of pH on Phe coprecipitation with various LDH precipitates: (■) Mg–Al, (□) Mn–Al, (●) Ni–Al, (○) Zn–Al, and (◆) Zn–Cr.

TABLE 1
Chemical Compositional Data of Solid Products

M^{2+}–M^{3+}	pH	M^{2+}/M^{3+}	NO_3/M^{3+}	Phe/M^{3+}	XRD phase obtained
Mg–Al	10	2.03	0.46	0.42	LDH
Mn–Al	9	2.33	0.57	0.80	LDH
Ni–Al	8	1.86	0.34	1.00	LDH + HDS[a]
Zn–Al	8	2.33	0.57	0.83	LDH
Zn–Cr	9	2.03	0.49	0.64	LDH

[a] HDS: hydroxy double salt.

products are indicated in Table 1. The molar ratio M^{2+}/M^{3+} was 1.86–2.33 in all the LDH systems. However, the total number of intercalated Phe and NO_3^- ions was inconsistent with the positive charge of the LDH basal layer, if Phe is assumed to exist in anion form. The theoretical intercalation capacity (TIC) of LDH is 1.00 mol/mol of M^{3+} for a univalent anion. The (Phe + NO_3^-)/M^{3+} molar ratio was estimated at 1.13–1.40 mol/mol of M^{3+} namely, more Phe and NO_3^- ions than TIC were contained in the Phe/Mn–Al, Ni–Al, Zn–Al and Zn–Cr LDHs. Therefore, this result supports the belief that a large fraction of Phe is intercalated into the LDHs in amphoteric ion form. In the Mg–Al system, the degree of Phe coprecipitation reached a maximum at pH 10. It was, however, lower than that in the other LDH systems because most of the Phe is presented in anion form in the pH 10–12 range. In general, LDHs are easy to intercalate, the anion having high charge density in their interlayer space. Accordingly, the coexisting anions, i.e., OH^- and NO_3^- ions, are more predominantly intercalated than anionic Phe. The degree of Phe coprecipitation decreased with increasing solution pH because the amount of OH^- ion in the solution increased. Further, the molar ratio (Phe + NO_3^-)/Al^{3+} became 0.88, and the numbers of intercalated anionic Phe and NO_3^- ion were lower than the number of TIC. The remaining positive charge of the LDH basal layer is thought to be neutralized by the coexistent OH^- ion. As a result, Phe was coprecipitated in amphoteric and/or anion form with the various LDH precipitates.

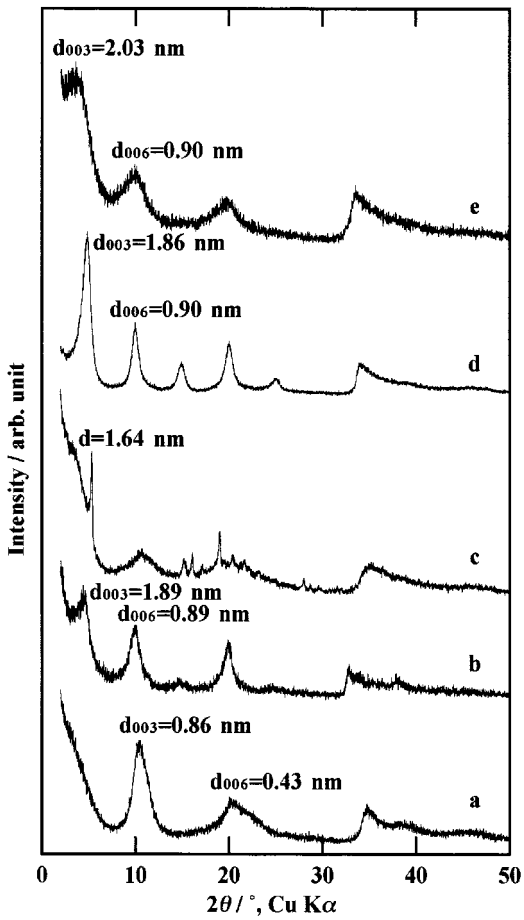

FIG. 2. XRD patterns of solid products: (a) Mg–Al (pH 10), (b) Mn–Al (pH 9), (c) Ni–Al (pH 8), (d) Zn–Al (pH 8), and (e) Zn–Cr (pH 9) systems.

Characterization of Solid Products

The resulting solid products are designated as Phe/M^{2+}–M^{3+} LDH (coprecipitation pH value) in this paper.

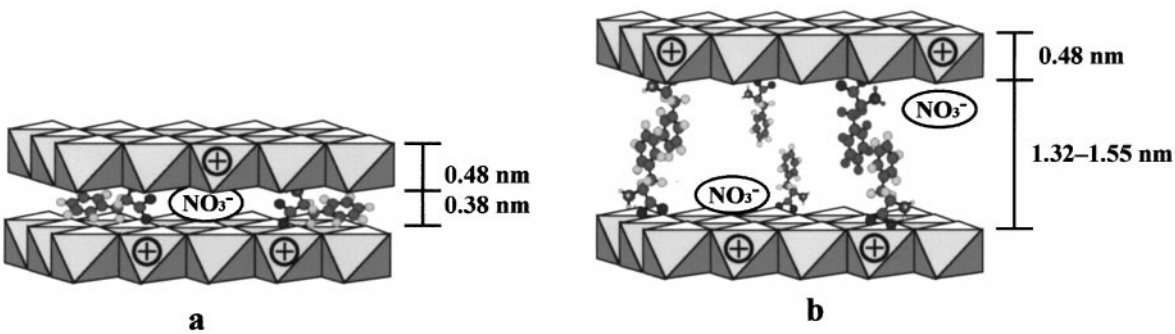

FIG. 3. Schematic models of the intercalation of Phe into various LDHs. (a) Mg–Al (pH 10) LDH, (b) Mn–Al (pH 9), Zn–Al (pH 8), and Zn–Cr (pH 9) LDHs.

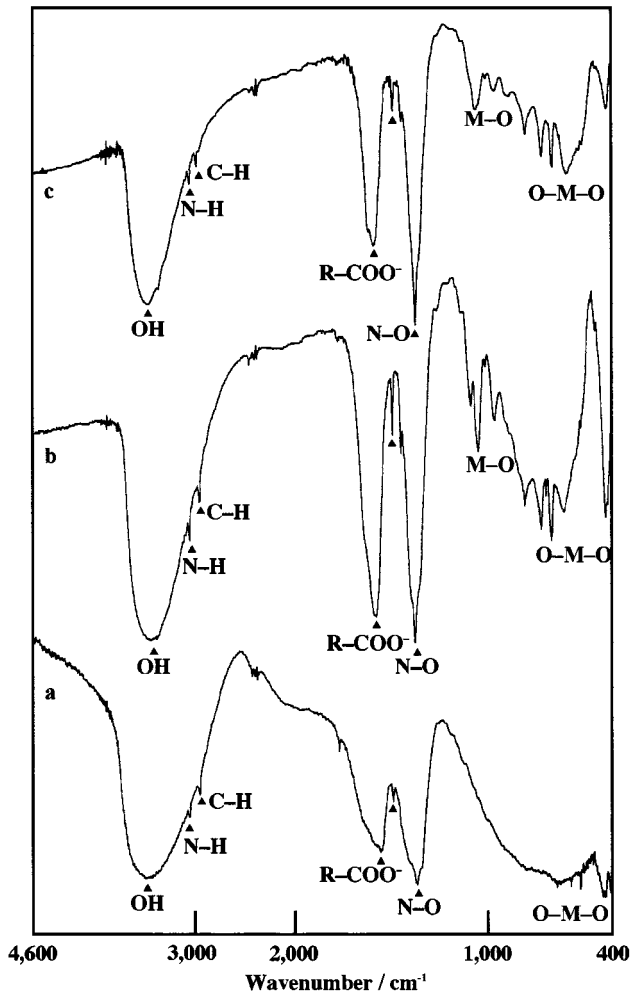

FIG. 4. FT-IR spectra of Phe/LDHs: (a) Mg–Al (pH 10), (b) Mn–Al (pH 9), and (c) Zn–Al (pH 8) systems.

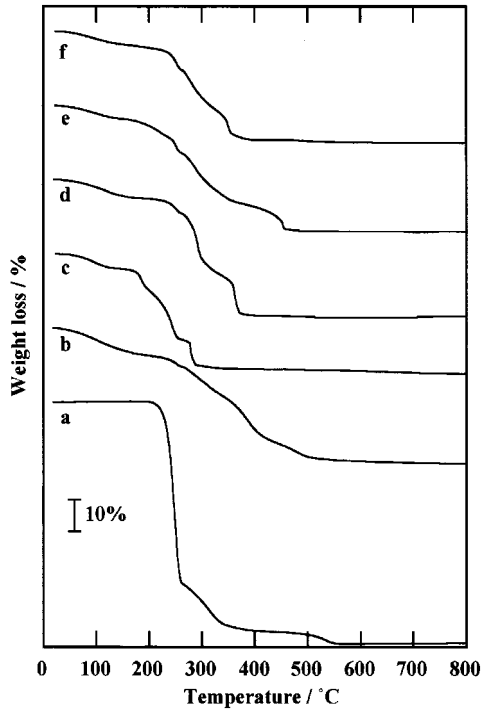

FIG. 5. TG curves of various Phe/LDH precipitates. (a) Phe, (b) Mg–Al (pH 10), (c) Mn–Al (pH 9), (d) Ni–Al (pH 8), (e) Zn–Al (pH 9), and (f) Zn–Cr (pH 9) LDHs.

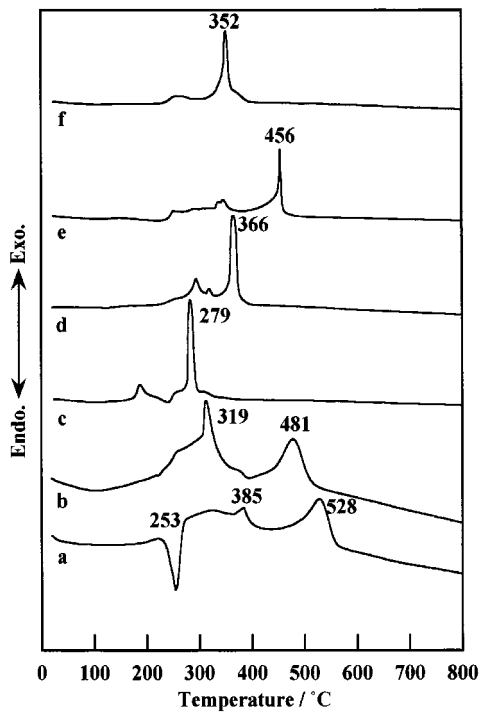

FIG. 6. DTA curves of various Phe/LDH precipitates: (a) Phe, (b) Mg–Al (pH 10), (c) Mn–Al (pH 9), (d) Ni–Al (pH 8), (e) Zn–Al (pH 9), and (f) Zn–Cr (pH 9) LDHs.

The XRD patterns of the solid products are presented in Fig. 2. The main diffraction peaks with LDH structure ($d_{003} = 0.86$ nm and $d_{006} = 0.43$ nm) are observed for the Phe/Mg–Al LDH (pH 10) in Fig. 2a, indicating that anionic Phe and NO_3^- ions are intercalated in the interlayer space. As the thickness of the LDH hydroxide basal layer is 0.48 nm, the interlayer space is calculated as 0.38 nm. The molecular size of Phe is 0.88 nm in length and 0.31 nm in thickness. On the basis of these data, a schematic model of the Phe/Mg–Al (pH 10) LDH is shown in Fig. 3a. The expanded interlayer space indicates that the anionic Phe is horizontally oriented and the NO_3^- ion is vertically oriented for the LDH basal layer. In general, the main diffraction peaks ($d_{003} = 0.88$ nm and $d_{006} = 0.44$ nm) are observed in the NO_3/Mg–Al LDH. The difference in the basal spacing ($\Delta d_{003} = 0.02$ nm) of the Phe/Mg–Al LDH is due to the negative charge of the guest anionic Phe, which is intercalated by the electrostatic force of attraction between the

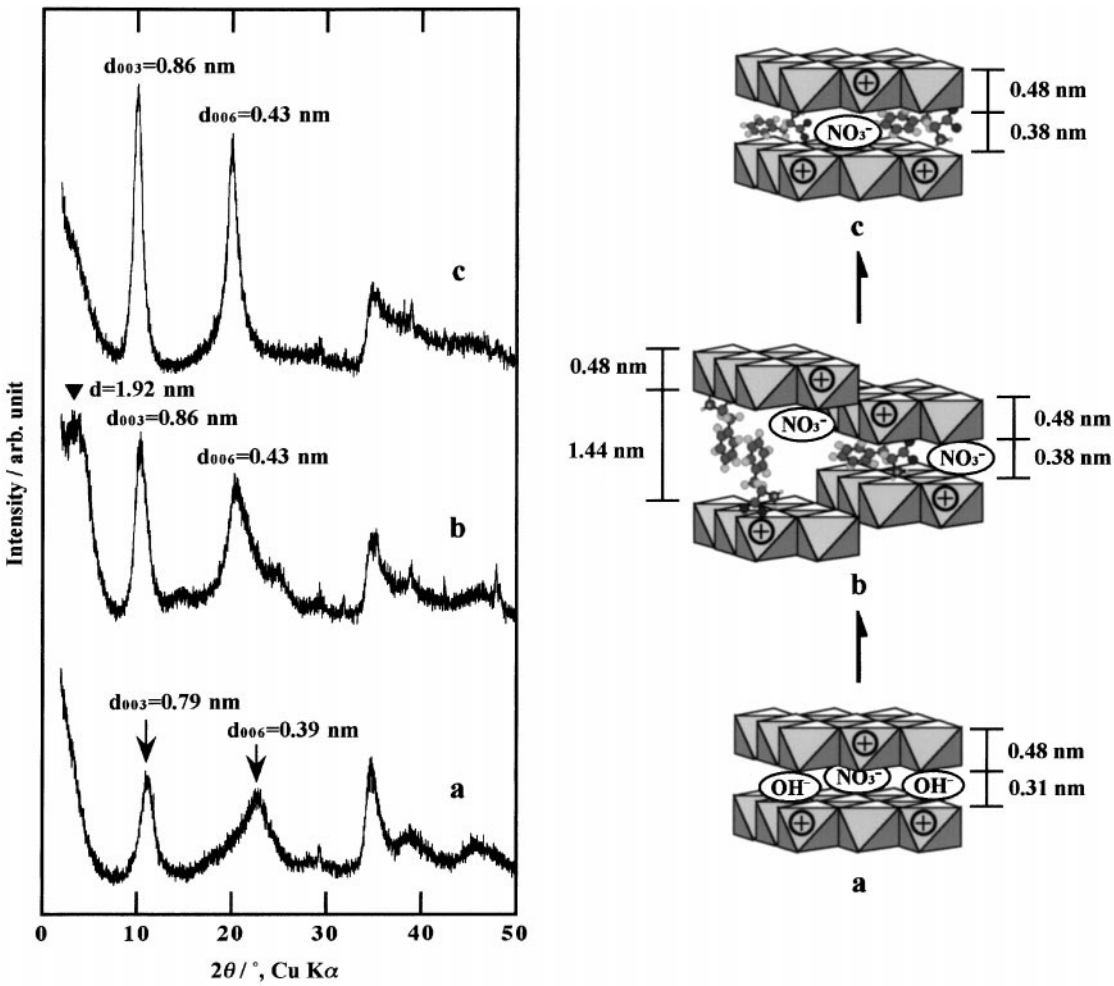

FIG. 7. XRD patterns and schematic models of the formation process of Phe/Mg–Al LDH (pH 10) precipitate. Precipitate after 3 min (a), 10–25 min (b), and final precipitate (c).

anionic Phe and LDH basal layer. The XRD patterns of solid products (Mn–Al (pH 9), Zn–Al (pH 8), and Zn–Cr (pH 9)) are shown in Figs. 2b, 2d, and 2e. The LDH crystallinity was lower in both the Phe/Mn–Al (pH 9) and Zn–Cr (pH 9) LDHs, while it was quite higher in the Phe/Zn–Al LDH. The diffraction peaks with the expanded LDH structure ($d_{003} = 1.89$, 1.86, and 2.03 nm) are observed in Phe/Mn–Al (pH 9), Zn–Al (pH 8), and Zn–Cr (pH 9) LDHs, from which the interlayer spaces are calculated as 1.41, 1.38, and 1.55 nm, respectively. Although these values are larger than the molecular size of Phe, the expanded interlayer spaces demonstrate the intercalation of Phe into the LDHs interlayer space. A schematic representation of the Phe/Mn–Al, Zn–Al, and Zn–Cr LDHs are shown in Fig. 3b. As a possible model, bilayer Phe is considered to orient vertically to the LDH basal layer, in which the Phe side chain is overlapped by hydrophobic interaction, namely, π–π overlap of the phenyl groups.

In the Ni–Al system (pH 8), the solid product hardly has a distinct LDH structure in spite of the high degree of Phe coprecipitation. A sharp diffraction peak ($d = 1.64$ nm), which is due to the formation of the layered Phe/Ni(OH)$_2$ composite (hydroxy double salt: HDS) (31) is shown in Fig. 2c. However, two broad peaks ($d = 2.00$ and 0.80 nm) are slightly observed, which are probably assigned to the LDH structure. Accordingly, the resulting solid product was a mixture of LDH and HDS in the Ni–Al system.

The FT-IR spectra of the Phe/Mg–Al, Mn–Al, and Zn–Al LDHs are shown in Fig. 4. The weak absorption peaks of the alkyl C–H stretch and amine N–H stretch are observed in the 3030 to 2900 cm^{-1} region, and the strong absorption peaks of R–COO$^-$ antisymmetric and symmetric stretches at 1590 and 1400 cm^{-1} are observed, respectively. These peaks demonstrated that Phe was intercalated into the LDHs. The co-intercalated NO_3^- ion gives a very strong absorption peak at 1385 cm^{-1}. A broad absorption peak in

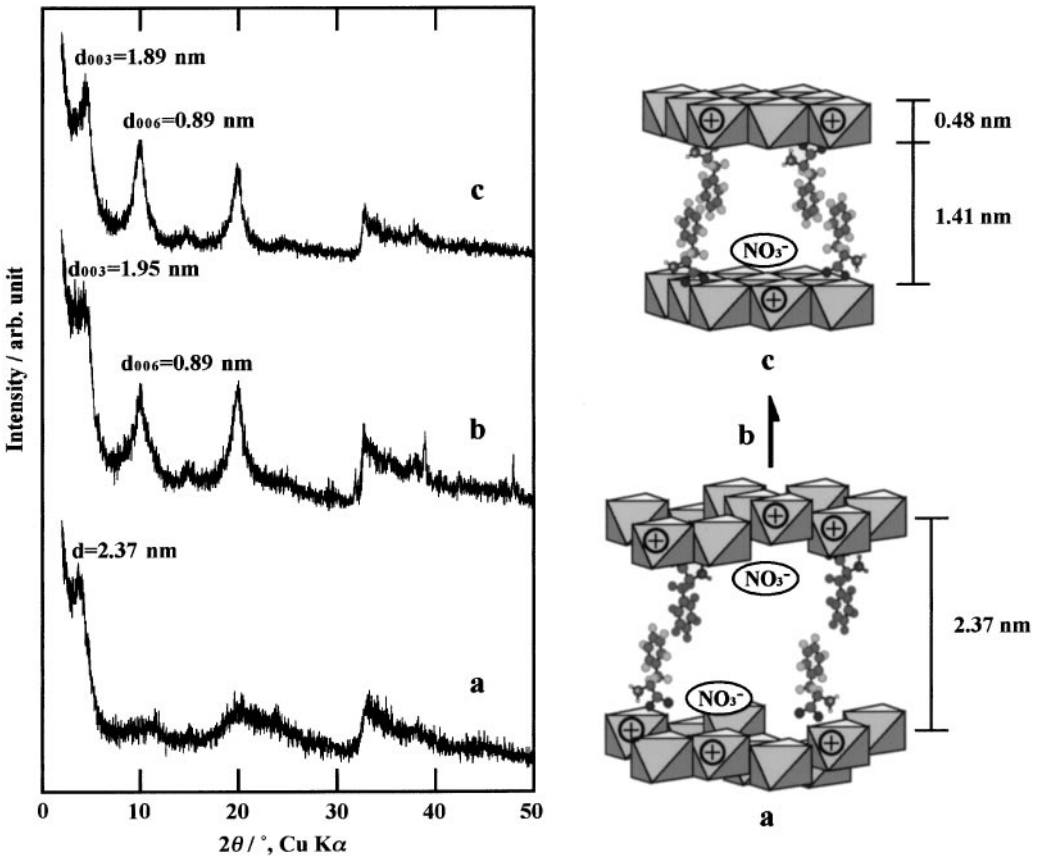

FIG. 8. XRD patterns and schematic models of the formation process of Phe/Mn–Al LDH (pH 9) precipitate. Precipitate after 3 min (a), 20 min (b), and final precipitate (c).

the region 3600–3000 cm^{-1} is assigned to O–H group stretches of both the hydroxide basal layer and interlayer water. In the low-frequency region, the absorption peaks of the spectra that correspond to the lattice vibration modes are attributed to M–O (840 and 650 cm^{-1}) and O–M–O (430 cm^{-1}) vibrations.

The TG curves of the Phe/M^{2+}–M^{3+} LDHs are represented in Fig. 5. In the case of Phe as a reference sample (Fig. 5a), three weight losses due to the decomposition of Phe in the temperature range 200–253°C (weight loss 70%) and two-step combustion of Phe are observed in the temperature ranges 253–385°C (weight loss 20%) and 385–528°C (weight loss 10%). On the other hand, the thermal decomposition of the Phe/M^{2+}–M^{3+} LDHs was influenced by the kind of LDH components (Figs. 5b–5f). Total weight loss of the Phe/M^{2+}–M^{3+} LDHs was about 50% and a major weight loss indicated three steps the same as those of Phe. The first step corresponding to the removal of adsorbed water and interlayer water was observed for all the Phe/M^{2+}–M^{3+} LDHs from room temperature to 250°C. The second step due to both the dehydroxylation of the LDH basal layer in the temperature region 250–450°C and the decomposition of the intercalated Phe between 200 and 250°C was observed. The third step corresponding to the combustion of the intercalated Phe was followed in the temperature region 270–480°C, which differed by the kind of metal ions in the LDH basal layer. In particular, the combustion weight loss of the intercalated Phe was observed at 279°C on the Phe/Mn–Al LDH. This temperature was the lowest in all the Phe/M^{2+}–M^{3+} LDHs, which suggests that the Mn–Al LDH possesses the best catalytic action for the decomposition of the guest organic compounds in the LDH interlayer gallery.

The DTA curves of the Phe/M^{2+}–M^{3+} LDHs are shown in Fig. 6. In the case of Phe as a reference sample (Fig. 6a), an endothermic peak at 253°C for the decomposition of Phe and two exothermic peaks at 385 and 528°C for the combustion of Phe are observed. In the case of the Phe/M^{2+}–M^{3+} LDHs, the combustion of the intercalated Phe is shown in the main exothermic peaks in the temperature region 280–480°C, which are lower than the combustion temperature of Phe itself, especially in the Phe/Mn–Al LDH.

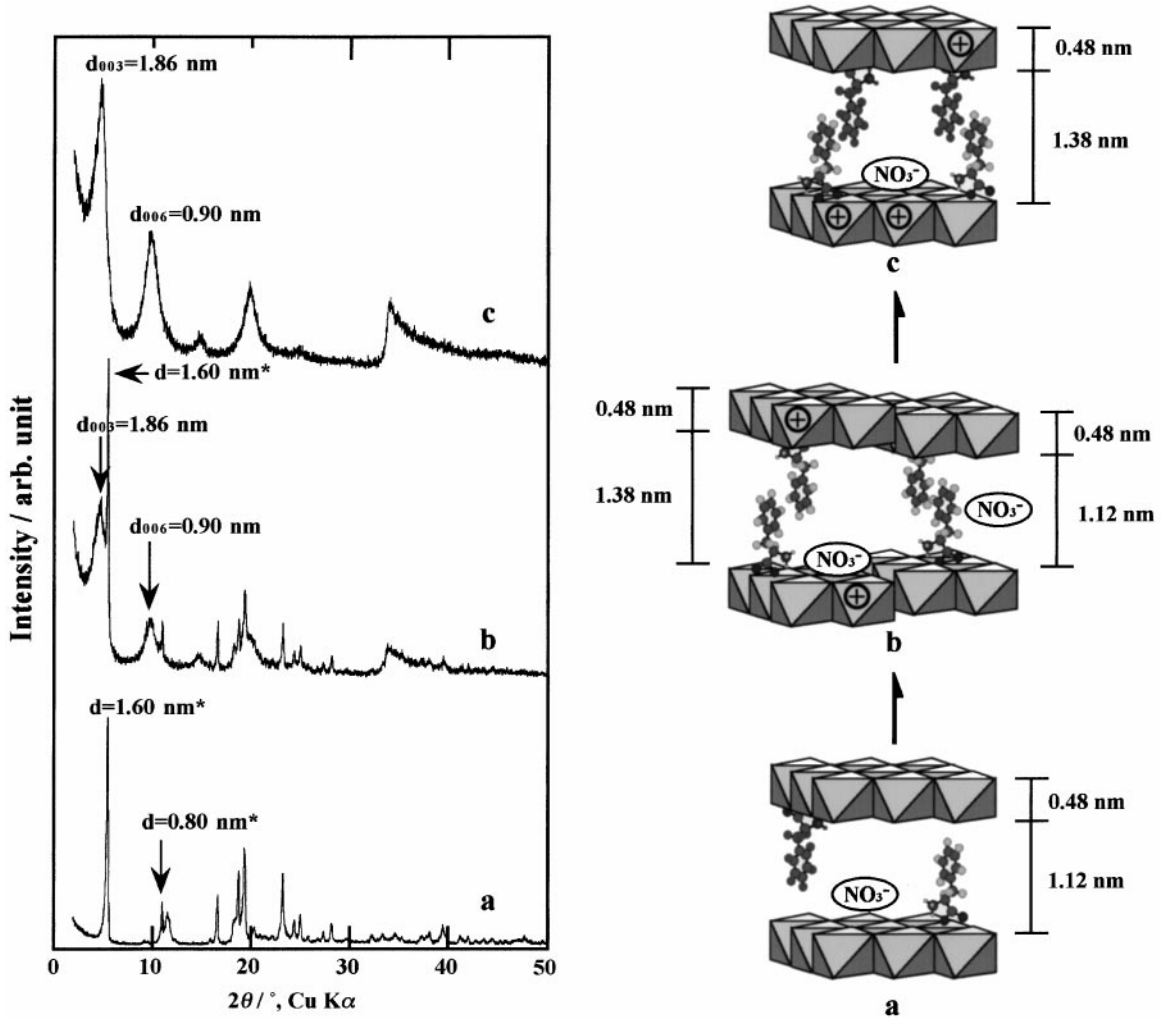

FIG. 9. XRD patterns and schematic models of the formation process of Phe/Zn–Al LDH (pH 8) precipitate. Precipitate after 3 min (a), 30 min (b), and final precipitate (c). *Phe/$Zn(OH)_2$ composite.

Formation Process of Phe/LDHs Precipitates

In this section, the formation of the Phe/Mg–Al, Mn–Al, and Zn–Al LDH precipitates has also been investigated. The XRD patterns and schematic models for the formation of the Phe/Mg–Al LDH (pH 10) precipitate are observed in Fig. 7. In the initial stage, the distinct diffraction peaks ($d_{003} = 0.79$ nm and $d_{006} = 0.39$ nm) with the LDH structure may already be observed in Fig. 7a. These values indicate that NO_3^- and/or OH^- ions are initially intercalated into the LDH interlayer space (Fig. 7a). In the transitional stage, the expanded LDH structure with broad diffraction peaks ($d_{003} = 0.86$ nm and $d = 1.92$ nm) are observed in Fig. 7b. This expanded interlayer space suggests the occurrence of the intercalation of Phe into the Mg–Al LDH. Thus, anionic Phe substitutes for NO_3^- and/or OH^- ions by ion-exchange reaction and is temporarily oriented vertically with respect to the basal layer by hydrophobic interaction of Phe (Fig. 7b). In the final stage, the main diffraction peaks ($d_{003} = 0.86$ nm and $d_{006} = 0.43$ nm) are observed in Fig. 7c, which correspond to the basal spacing of the anionic Phe and NO_3^- ion intercalated LDH as in Fig. 2a. As a result, the intercalated Phe was rearranged by the electrostatic force of attraction between the LDH basal layer and anionic Phe in the two-dimensional space of the Mg–Al LDH.

Figure 8 shows the XRD patterns and schematic models for the formation of the Phe/Mn–Al LDH (pH 9) precipitate. A broad diffraction peak ($d = 2.37$ nm) in Fig. 8a indicates that Phe is randomly intercalated into the Mn–Al LDH with low crystallinity in the initial stage. With elapsed reaction time, the crystallinity of LDH increased as shown in Fig. 8b, and the main diffraction peak shifted to higher angles. In the final stage, the Phe/Mn–Al LDH possesses

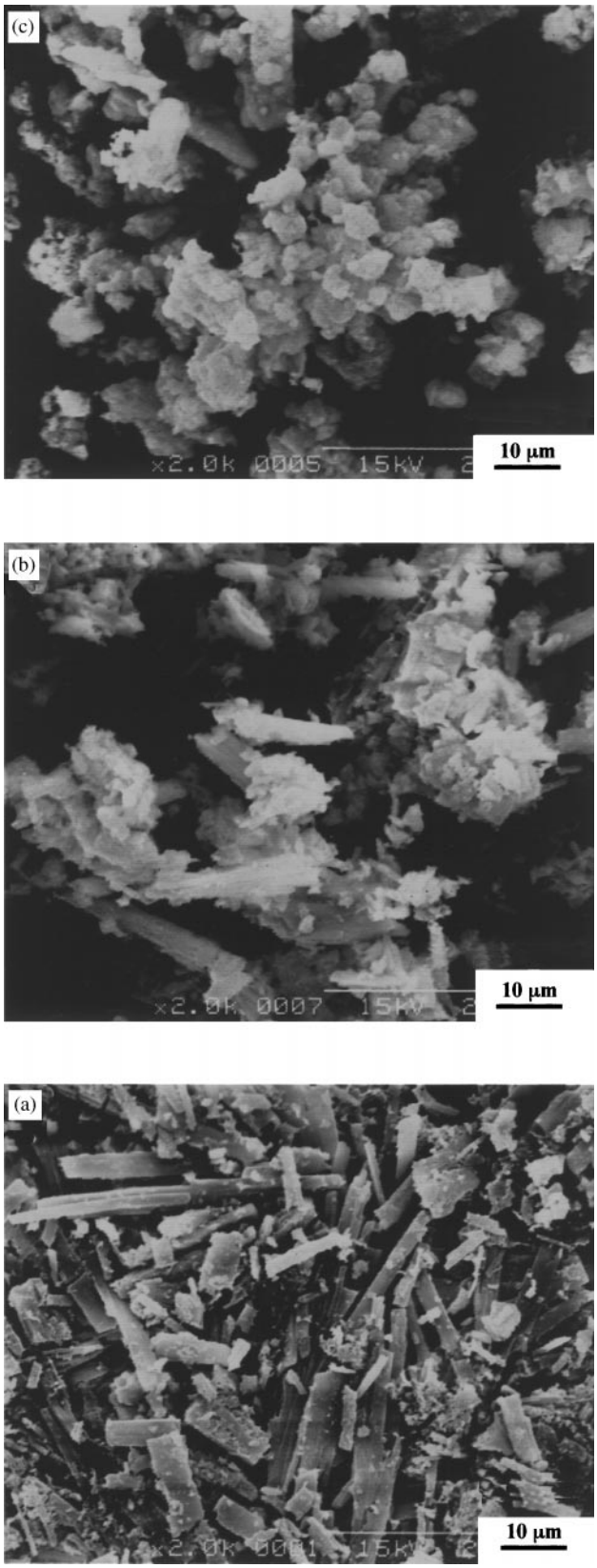

FIG. 10. SEM images of Phe/Zn–Al (pH 8) LDH precipitate obtained after 3 min (a), 30 min (b), and final precipitate (c).

a well-crystallized LDH structure in which the diffraction peaks ($d_{003} = 1.89$ nm and $d_{006} = 0.89$ nm) are observed (in Fig. 8c).

The XRD patterns and schematic models for the formation process of the Phe/Zn–Al LDH (pH 8) precipitate are shown in Fig. 9. In the initial stage, the intensive diffraction peaks ($d = 1.60$ and 0.80 nm) are observed with a layered structure in Fig. 9a. These peaks are thought to be dependent on the formation of the layered $Zn(OH)_2$ composite. In the transitional stage, the other broad diffraction peaks ($d = 1.86$ and 0.90 nm) are also observed with the diffraction peaks of the Phe/$Zn(OH)_2$ composite in Fig. 9b. This result indicates that the mixture of the Phe/Zn–Al LDH and Phe/$Zn(OH)_2$ composites formed in the transitional stage. In the final stage, the solid product has an expanded LDH structure ($d_{003} = 1.86$ nm and $d_{006} = 0.90$ nm), as shown in Fig. 9c. The SEM images of the formation process of the Phe/Zn–Al LDH are shown in Fig. 10. The solid product has a rod-like morphology ca. 15 μm in length in the initial stage in Fig. 10a. In general, the LDH crystal has a plate-like morphology and a hexagonal crystallite. The crystal with rod-like morphology is the Phe/$Zn(OH)_2$ composite; namely, the hydroxide basal layer was hardly substituted for the Al^{3+} ion in the initial stage. In Fig. 10b, the solid product has rod-like and plate-like (hexagonal crystallite) morphologies in the transitional stage. In the final stage, the solid product has only the plate-like morphology and is the hexagonal crystallite in Fig. 10c. This morphology agrees with the characteristics of LDH crystallite. Thus, XRD patterns and SEM images indicated that Phe/Zn–Al LDH formed via three stages.

Intercalation of Various Amino Acids for Zn–Al LDH

So far, we have disclosed that the Zn–Al system was the most suitable LDH component for the intercalation of amino acid by coprecipitation. In this section, the intercalation of various amino acids into LDH has been investigated by the same method using the Zn–Al system (amino acid/Zn/Al molar ratio = 2/1/1 and solution pH 8). The degrees of coprecipitation of various amino acids are presented in Table 2. It was found that they were strongly influenced by the kind of sidechains of the amino acids. For neutral amino acids, a high degree of coprecipitation was generally obtained. In the case of the amino acids having an aromatic group such as Phegly, Trp, and Tyr, the degree of coprecipitation was 53, 82, and 77%, and the basal spacing of these amino acid/LDHs was 1.91, 1.89, and 1.77 nm, respectively. These values indicate that amino acids are intercalated into the LDH interlayer with overlapping aromatic groups by hydrophobic interaction between sidechains as in Phe/Zn–Al LDH (Fig. 3b). In the case of the amino acids having an aliphatic group, such as Gly, Ala, α-ABA, Norval, Val, Norleu, Leu, and Ile, the degree of

TABLE 2
The Degree of Various Amino Acid Coprecipitation and XRD Data for Solid Products

Amino acid		Degree of amino acid coprecipitation (%)	d_{003} (nm)	Gallery height (nm)	Carbon number of sidechain
Glycine	(Gly)	11	0.90	0.42	0
Alanine	(Ala)	3	0.88	0.40	1
β-Alanine	(β-Ala)	2	0.89	0.41	1
α-Amino butyric acid	(α-ABA)	2	0.89	0.41	2
β-Amino butyric acid	(β-ABA)	1	0.88	0.40	2
γ-Amino butyric acid	(γ-ABA)	0	0.89	0.41	2
Norvaline	(Norval)	59	1.45	0.97	3
Valine	(Val)	4	0.88	0.40	3
Norleucine	(Norleu)	89	1.62	1.14	4
Leucine	(Leu)	65	1.45	0.97	4
Isoleucine	(Ile)	11	0.89	0.41	4
Phenylalanine	(Phe)	80	1.86	1.38	
Phenylalanine	(Phe)[29]	—	1.80	1.32	
Phenylglycine	(Phegly)	53	1.91	1.43	
Tryptophan	(Trp)	88	1.89	1.41	
Tyrosine	(Tyr)	72	1.77	1.29	
Tyrosine	(Tyr)[29]	—	1.75	1.27	
Arginine	(Arg)	9	0.89	0.41	
Histidine	(His)	42	2.00	1.52	
Aspartic acid	(Asp)	48	1.21	0.73	
Aspartic acid	(Asp)[28]	—	1.11	0.63	
Glutamic acid	(Glu)	41	1.28	0.80	
Glutamic acid	(Glu)[28]	—	1.19	0.71	

Note. Superscripted numbers in column two denote references from which data were obtained.

coprecipitation was influenced by the structure and carbon number of the side chain and increased with increasing carbon number of the sidechain. In the case of amino acids having a long alkyl group such as Norval, Norleu, and Leu, the degree of coprecipitation was 59, 89, and 65%, and the basal spacing of these amino acid/LDHs was 1.45, 1.62, and 1.45 nm, respectively. Norval and Val and Norleu, Leu, and Ile are structural isomers. However, it should be noticed that Val and Ile were hardly coprecipitated with the Zn–Al LDH precipitate. This result suggests the possibility that amino acid coprecipitation is related to hydrophobic interaction among amino acid sidechains. Hence, the degrees of Gly, Ala, and α-ABA coprecipitation were considerably lower, because these amino acids have shorter sidechains. On the other hand, the degree of coprecipitation of basic amino acids, Arg ($pK_1 = 1.82$, $pK_2 = 8.99$, and $pK_R = 12.48$) and His ($pK_1 = 1.80$, $pK_2 = 9.33$, and $pK_R = 6.04$), was 9 and 42%, respectively. At pH 8, most of the Arg and His existed as a cation and an amphoteric ion. In particular, Arg was difficult to intercalate into Zn–Al LDH due to the repulsion of positive charge occurring between the LDH basal layer and the sidechain of Arg. In contrast, acidic amino acids, Asp and Glu, existing in monovalent anion form were easily intercalated by the electrostatic force of attraction between the anionic amino acid and the LDH basal layer at pH 8. Moreover, β- and γ-amino acids failed to be intercalated into the Zn–Al LDH. It can be said that LDH has a preferential intercalation ability for α-amino acids.

The XRD patterns of the solid products are shown in Fig. 11. In the case of the hydrophobic amino acids, expanded basal spacings (Phegly/LDH $d_{003} = 1.91$ nm and Tyr/LDH $d_{003} = 1.89$ nm) are observed in Figs. 11b and 11c. Despite lower crystallinity, the His/LDH has a layered structure, and broad diffraction (ca. 2.00 nm) is observed in Fig. 11d. The diffraction peaks (Asp/LDH $d_{003} = 1.21$ nm and Glu/LDH $d_{003} = 1.28$ nm) with the distinct expanded LDH structure are shown in Figs. 11e and 11f. These values indicate that the intercalated Asp and Glu were oriented vertically for the LDH basal layer with cross-linking the LDH layers by their carboxylate groups. So far, it has been reported that the basal spacing of the Asp and Glu/Mg–Al LDH was expanded to 1.11 and 1.19 nm, respectively. The difference in the basal spacing (ca. 0.10 nm) between the

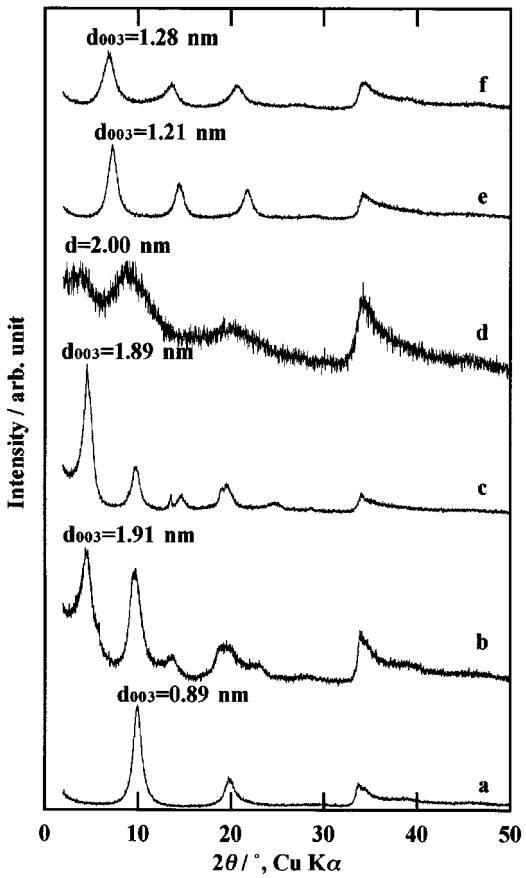

FIG. 11. XRD patterns of amino acid/Zn–Al LDH precipitates. (a) Gly, (b) Phegly, (c) Trp, (d) His, (e) Asp, and (f) Glu.

Zn–Al LDH and Mg–Al LDH was assumed to depend on the charge number of the intercalated acidic amino acids. In a comparison of the Asp and Glu/Mg–Al LDHs with the Asp and Glu/Zn–Al LDHs, the amino acids in the former exist in divalent anion form at pH 12, while those in the latter are present in monovalent anion form at pH 8. Consequently, the basal layer of the Zn–Al LDH was more expanded than that of the Mg–Al LDH.

CONCLUSIONS

Phe was coprecipitated with the various LDH precipitates in amphoteric ion form in the Mn–Al, Ni–Al, Zn–Al and Zn–Cr systems and in anion form in the Mg–Al system. The degree of Phe coprecipitation was influenced by the solution pH and the kind of LDH system. As a possible model, Phe was vertically arranged in the Mn–Al, Zn–Al, and Zn–Cr systems and horizontally presented in the Mg–Al for the LDH basal layer. In Ni–Al systems, the resulting solid product was the mixture of LDH and HDS. Furthermore, the thermal decomposition of the intercalated Phe was accelerated by a catalytic action of metal ions in the host hydroxide layer, especially in the Mn–Al system. This catalytic action of the host hydroxide layer will be applied to the decomposition of harmful organic compounds. The formation process of the Phe/Mg–Al, Mn–Al, and Zn–Al LDHs precipitates was also found to be different in the kind of LDH systems. Then, the coprecipitation behavior of various amino acids was influenced by the kind of sidechain of amino acids. In particular, α-amino acids having a hydrophobic sidechain were preferentially intercalated into the LDH interlayer in amphoteric ion form. In future, the formation of the amino acids/LDHs may be used in separation and decomposition techniques and synthesis of novel organic–inorganic hybrid material.

ACKNOWLEDGMENT

This research has been supported partially by a grant from the Foundation for Japanese Chemical Research.

REFERENCES

1. A. De Roy, *Mol. Cryst. Liq. Cryst.* **311,** 173 (1998).
2. S. Miyata, *Clays Clay Miner.* **28,** 50 (1980).
3. F. Cavani, F. Tirifiro, and A. Vaccari, *Catal. Today* **11,** 173 (1991).
4. K. Kuma, W. Paplawsky, B. Gedulin, and G. Arrhenius, *Origin Life* **19,** 573 (1989).
5. R. Allmann, *Acta Crystallogr. Sect. B* **24,** 972 (1967).
6. B. Sels, D. De Vos, M. Buntinx, F. Pierard, A. K. Mesmaeker, and P. Jacobs, *Nature* **400,** 855 (1999).
7. J. Qiu and G. Villemure, *J. Electroanal. Chem.* **428,** 165 (1997).
8. T. Kuwahara, H. Tagaya, J. Kadokawa, and K. Chiba, *J. Mater. Synth. Process.* **4,** 69 (1996).
9. T. Shichi, K. Takagi, and Y. Sawaki, *Clay Sci.* **10,** 503 (1999).
10. H. Zhao and G. F. Vance, *Clays Clay Miner.* **46,** 712 (1998).
11. H. Tagaya, H. Morioka, S. Ogata, M. Karasu, J. Kadokawa, and K. Chiba, *Appl. Surf. Sci.* **121,** 476 (1997).
12. S. Bonnet, C. Forano, A. De Roy, and J. P. Besse, *Chem. Mater.* **8,** 1962 (1996).
13. S. P. Newman and W. Jones, *New J. Chem.* **22,** 805 (1998).
14. M. A. Drezdzon, *Inorg. Chem.* **27,** 4628 (1988).
15. C. O. Oriakhi, I. V. Farr, and M. M. Lerner, *J. Mater. Chem.* **6,** 103 (1996).
16. C. O. Oriakhi, I. V. Farr, and M. M. Lerner, *Mater. Res. Soc. Symp. Proc.* **432,** 297 (1997).
17. H. Zhao and G. F. Vance, *J. Chem. Soc., Dalton Trans.*, 1961 (1997).
18. H. Nijs, A. Clearfield, and E. F. Vansant, *Microporous Mesoporous Mater.* **23,** 97 (1998).
19. W. Tseng, J. Lin, C. Mou, S. Cheng, S. Liu, P. P. Chu, and H. Liu, *J. Am. Chem. Soc.* **118,** 4411 (1996).
20. J. W. Boclair, P. S. Braterman, B. D. Brister, and F. Yarberry, *Chem. Mater.* **11,** 2199 (1999).
21. V. Prevot, C. Forano, and J. P. Besse, *J. Mater. Chem.* **9,** 155 (1999).
22. M. Kaneyoshi and W. Jones, *J. Mater. Chem.* **9,** 805 (1999).
23. M. Lakraimi, A. Legrouri, A. Barroug, A. De Roy, and J. P. Besse, *J. Mater. Chem.* **10,** 1007 (2000).
24. M. Meyn, K. Beneke, and G. Lagaly, *Inorg. Chem.* **29,** 5201 (1990).
25. E. Narita, T. Yamagishi, T. Kazuhara, O. Ichijo, and Y. Umetsu, *Clay Sci.* **9,** 187 (1995).
26. F. Kooli, I. C. Chisem, M. Vucelic, and W. Jones, *Chem. Mater.* **8,** 1969 (1996).

27. J. Choy, S. Kwak, J. Park, Y. Jeong, and J. Portier, *J. Am. Chem. Soc.* **121,** 1399 (1999).
28. N. T. Whilton, P. J. Vickers, and S. Mann, *J. Mater. Chem.* **7,** 1623 (1997).
29. Á. Fudala, I. Pálinkó, and I. Kiricsi, *Inorg. Chem.* **38,** 4653 (1999).
30. S. Aisawa, S. Takahashi, W. Ogasawara, Y. Umetsu, and E. Narita, *Clay Sci.* **11,** 317 (2000).
31. M. Meyn, K. Beneke, and G. Lagaly, *Inorg. Chem.* **32,** 1209 (1993).